Electronic Supplementary Material (ESI) for Inorganic Chemistry Frontiers.

3D-Printed square-hole electrode for dendrite-free Zinc-air Batteries

Chuancheng Mou[†‡], Yujia Bai[‡], Yi Zhang[†‡], Yijian Liu[‡], Zhen Hu[‡], Jiayu Chen[‡], Genxiang Wang[‡], Xuantao Wu[‡], Hui Wang[*§‡], Yuhan Sun[*†§‡]

[†]School of Physical Science and Technology, ShanghaiTech University, Shanghai, 201210, China

[§]Institute of Carbon Neutrality, ShanghaiTech University, Shanghai, 201210, China

[‡]Shanghai institute of Cleantech Innovation, Shanghai, 201616, China

Corresponding author:

* Yuhan Sun. e-mail: sunyh@sari.ac.cn

*Hui Wang. e-mail: wanghh@sari.ac.cn

1. Experimental Section

Chemical Reagents: Commercial 316L powder (Farsoon Technologies) with an average particle size of 15-53 μm was used to fabricate 3D-Printed architectures in this study. The Hydrochloric Acid (HCl, AR, 36-38 %), Nitric acid (HNO_3, GR, 65-68 %), Zinc sulfate heptahydrate ($ZnSO_4 \cdot 7H_2O$, AR), Potassium Hydroxide (KOH, RG) and Zinc Acetate ($C_4H_6O_4Zn$, RG) were purchased from Titan.

Preparation of 2D Fe-Ni and 3D Fe-Ni-X: Prior to the SLM process, the alloy power was dried in a drying oven at 80 ℃ to remove residual moisture. The metal alloy structure was prepared using a SLM machine (FS 273M) equipped with a IPG laser device with a maximum power output of 500 W and dynamic laser spot diameter of 80-100 μm. The SLM process was carried out in an Ar atmosphere with less than 0.35 % oxygen. In the cross-section of the specimens, the powder was set as the x-y plane exposed to the laser source. Finally, the 2D Fe-Ni and 3D Fe-Ni-X electrodes were fabricated. The experiment paraments for the SLM process with the 316L powder are given in **Table S1**. The thickness of both 2D and 3D electrodes is 1.6 mm. And the mass of the 2D electrode is 24.4647 g. The mass of 3D porous electrodes with pore sizes of 0.5 mm, 0.8 mm, 1.0 mm, 1.2 mm, and 1.5 mm were 21.3853 g, 19.8311 g, 18.9430 g, 16.8525 g, and 15.9954 g, respectively. It should be noted that no excessive reaction to the laser occurred, and the use of the 316L powder was found to be safe in the setup.

Preparation of 2D Fe//Ni-Zn and 3D Fe//Ni-Zn-X anodes: First, use detergent to clean the oil on the surface of the electrode. The dried 2D Fe-Ni and 3D Fe-Ni-X (0.5, 0.8, 1.0, 1.2, 1.5) electrodes were etched in mixed acid for 90 s to prepare 2D Fe-/Ni and 3D Fe-/Ni-X (0.5, 0.8, 1.0, 1.2, 1.5) electrodes. The etched electrodes were then ultrasonically cleaned with ultrapure water and anhydrous ethanol for 10 min, respectively. 2D Fe-Ni-Zn, 2D Fe//Ni-Zn, 3D Fe//Ni-Zn-X (0.5, 0.8, 1.0, 1.2, 1.5) zinc anodes were prepared by constant current (10 mA cm^{-2}) electrodeposition in $ZnSO_4$ (1 M) solution for 60 min with 2D/3D electrodes as working electrodes. The loading of zinc was 0.296 g.

Preparation of Air Cathode: Fe-Ni ANC@NSCA[1] bifunctional catalysts were used to facilitate the ORR and OER processes. Prepare catalyst slurry by mixing Fe-Ni ANC@NSCA bifunctional catalyst and carbon black into isopropanol. The homogeneously dispersed slurry is uniformly sprayed onto the nickel network. Leak-proofing of nickel mesh using breathable films. Finally, use a desktop paper cutter to cut it to the suitable size for use.

Assembled zinc air full batteries: The metal collector, air electrode, and zinc negative electrode are sealed and assembled into a zinc-air full cell in a clamp designed by the group. Subsequently, the reservoir, peristaltic pump and battery were connected. Finally, the electrolyte (9 M KOH, 0.25 M $C_4H_6O_4Zn$) is loaded into the reservoir.

Materials Characterization: The phase and crystal structure were recognized by X-ray diffraction (XRD, UltimalV) with Cu Kα (λ = 1.541866 Å) radiation in the range of 5-80 ° with a scanning rate of 10 ° min^{-1}. Sample morphology and elemental analysis

were obtained by scanning electron microscopy equipped with energy dispersive X-ray spectroscopy (EDX). The hydrophilicity of 2D/3D electrodes was tested using a contact angle tester.

Electrochemical Measurements: Long-life testing of full cells assembled with 2D/3D electrodes at a current density of 10 mA cm^{-2} was performed using the Blue Electric Test System. 2D Fe-Ni-Zn assembled into a full cell was used as a control group. CV testing of 2D/3D electrodes at different current densities (10, 12, 14, 16, 18, 20 mA cm^{-2}) using the Blue Electric Test System. LSV scan testing of 2D/3D electrodes using Princeton electrochemical workstation. EIS impedance testing of 2D/3D electrodes using Princeton electrochemical workstation.

Electric Current distribution: Ansys Fluent can model problems involving the electric potential field by solving the electric potential equation, which can be solved in both fluid and solid zones. The electric potential solver is automatically used with the built-in electrochemical reaction model allowing for the simulation of chemical and electrochemical reactions. The electric potential solver is also used in the Zinc-ion Battery model. When the electric potential solver is enabled, Ansys Fluent solves the following electric potential equation 1 (Eq. 1):

$$\nabla\cdot(\sigma\nabla\varphi)+S=0 \quad \text{(Eq. 1)}$$

where φ is the electric potential, σ is the electric conductivity in a solid zone or ionic conductivity in a fluid zone, and S is the source term.

Table S1 Experimental parameters for SLM of 316L powder.

Parameter	
Laser Power	210 W
Scanning Speed	900 mm/s
Layer Thickness	30 μm
Selected Laser	IPG laser (λ=1064 nm)
Substrate	304(273*273 mm)
Atmosphere	N_2(O_2<0.35 %)

Table S2 XRF elemental content testing of 3D porous electrodes before and after etching.

	Fe	Cr	Ni	Mo	Mn	Si	others
316 Lpowder (wt%)	Bal.	16.0-18.0	10.0-14.0	2.0-3.0	<2.0	<1.0	-
3D Fe-Ni-X	62.1	16.7	9.5	2.4	0.7	1.1	-
3D Fe//Ni-X	63.4	18.2	9.9	2.5	0.7	0.8	-

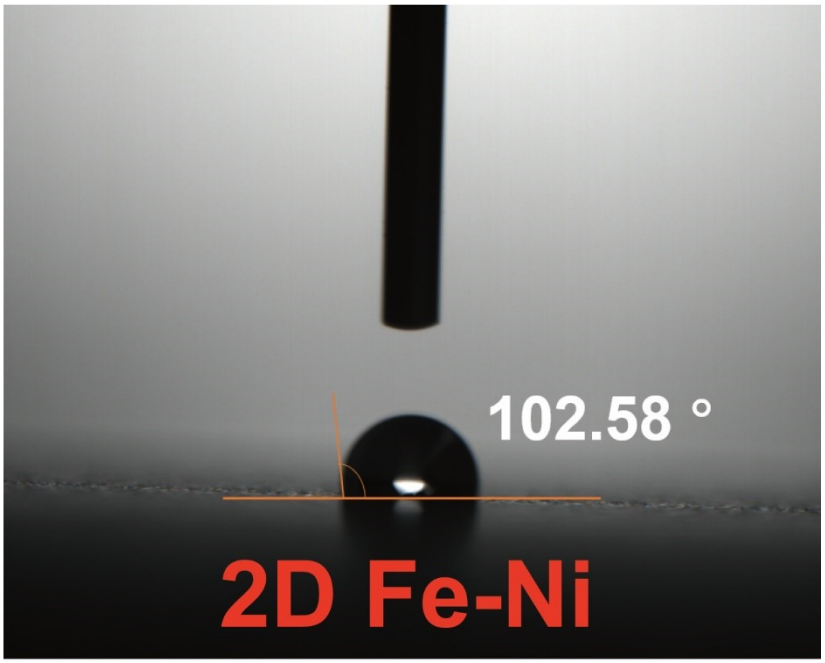

Figure S1 Wettability testing of 2D Fe-Ni electrodes.

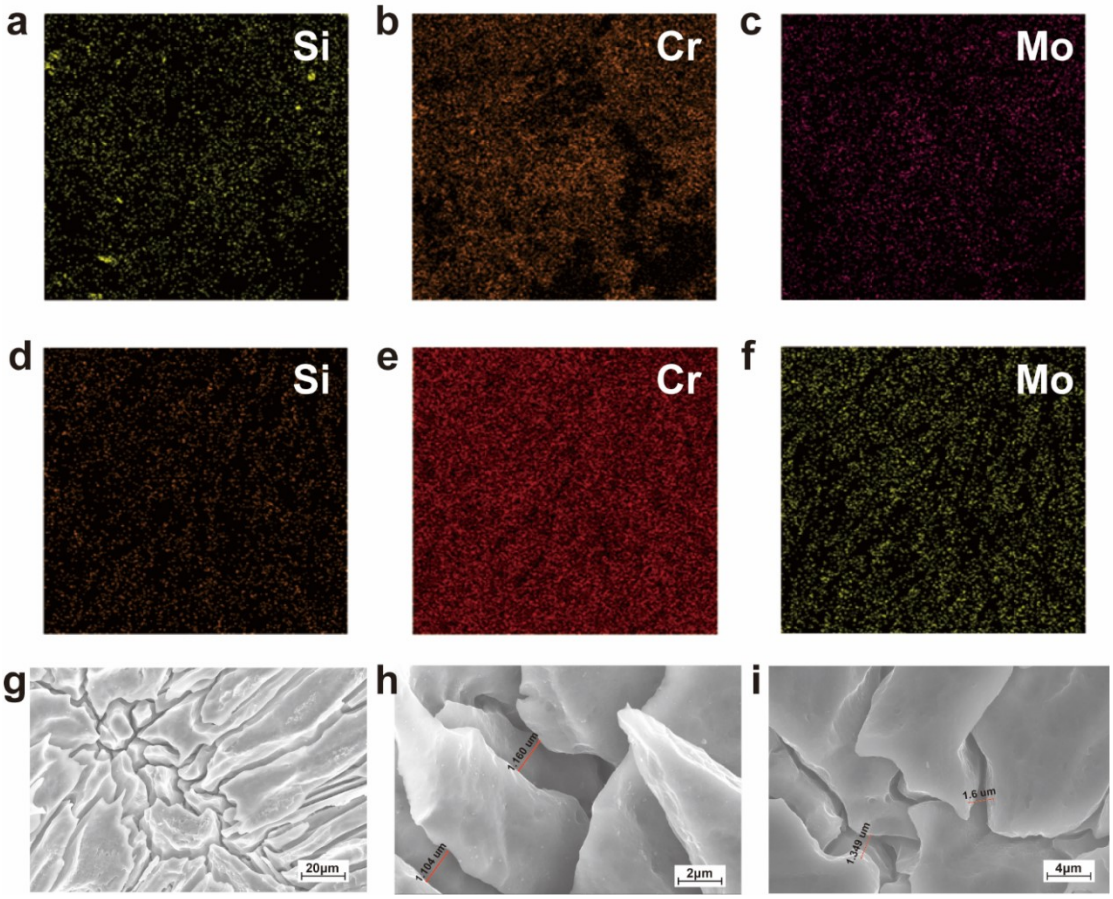

Figure S2 (a-c) EDX elemental distribution maps of 3D Fe-Ni-X. (d-f) EDX elemental distribution maps of 3D Fe//Ni-X. (g-i) SEM morphology of 3D Fe//Ni-X at different magnifications.

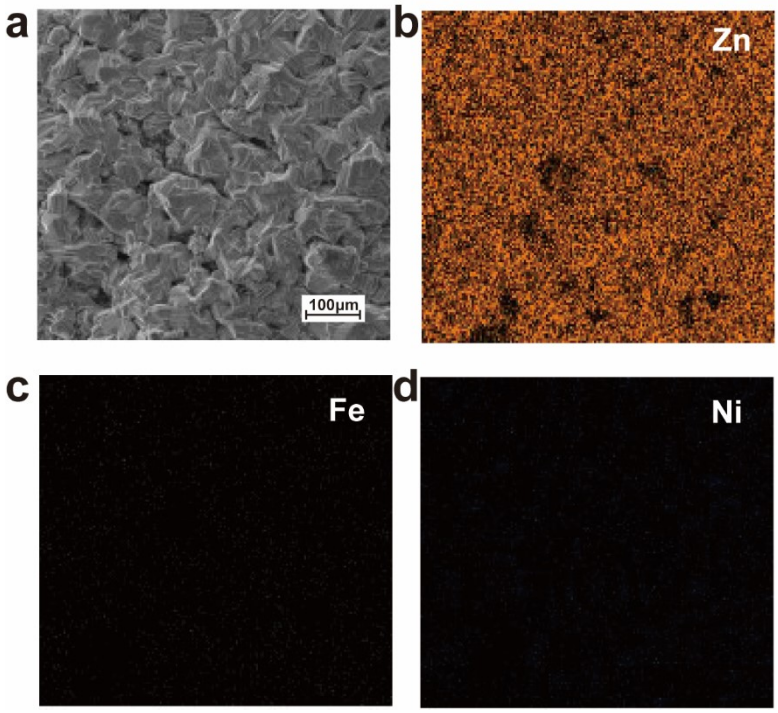

Figure S3 (a) SEM image of 3D Fe//Ni-Zn-X. (b-d) The EDX elemental distribution of Zn, Fe and Ni elements.

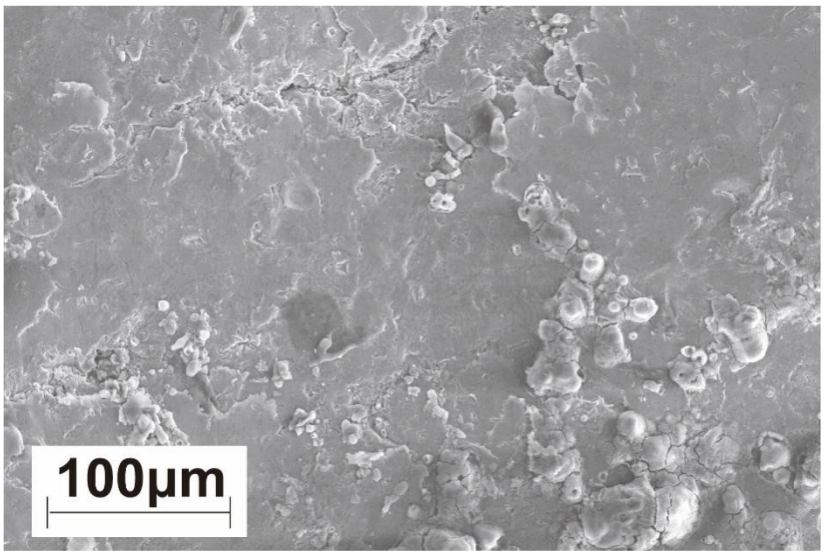

Figure S4 SEM with different magnifications of 2D Fe-Ni.

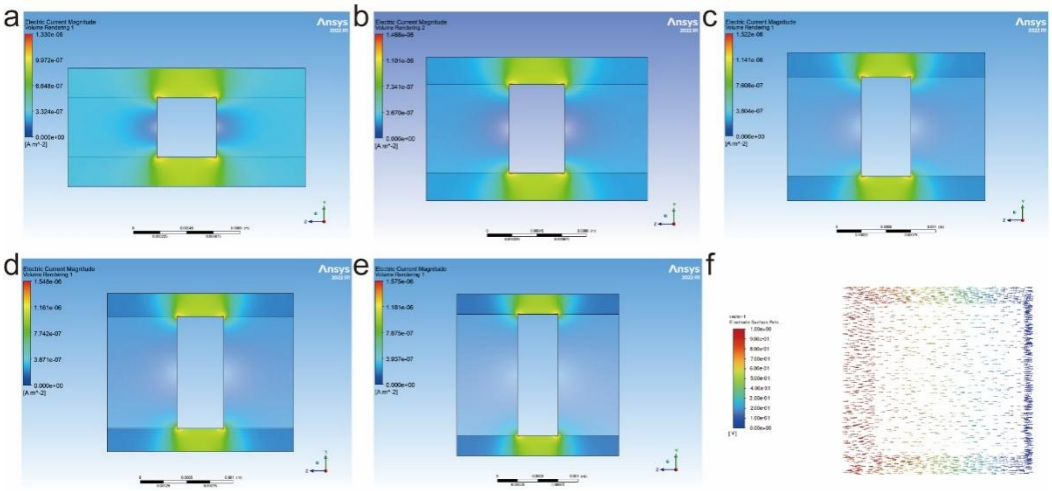

Figure S5 (a-e) Side views of current density distribution for (a) 3D Fe-Ni-0.5 electrode, (b) 3D Fe-Ni-0.8, (c) 3D Fe-Ni-1.0, (d) 3D Fe-Ni-1.2 and (e) 3D Fe-Ni-1.5, respectively. (f) Side view of the current flow distribution of the 2D Fe-Ni electrode.

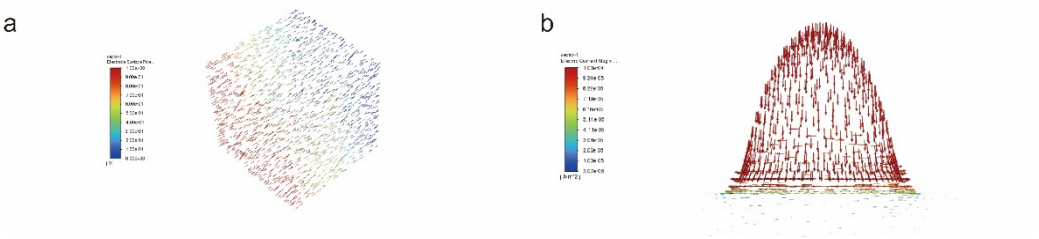

Figure S6 Current flow direction distribution (a, b) at the electrode surface protrusion.

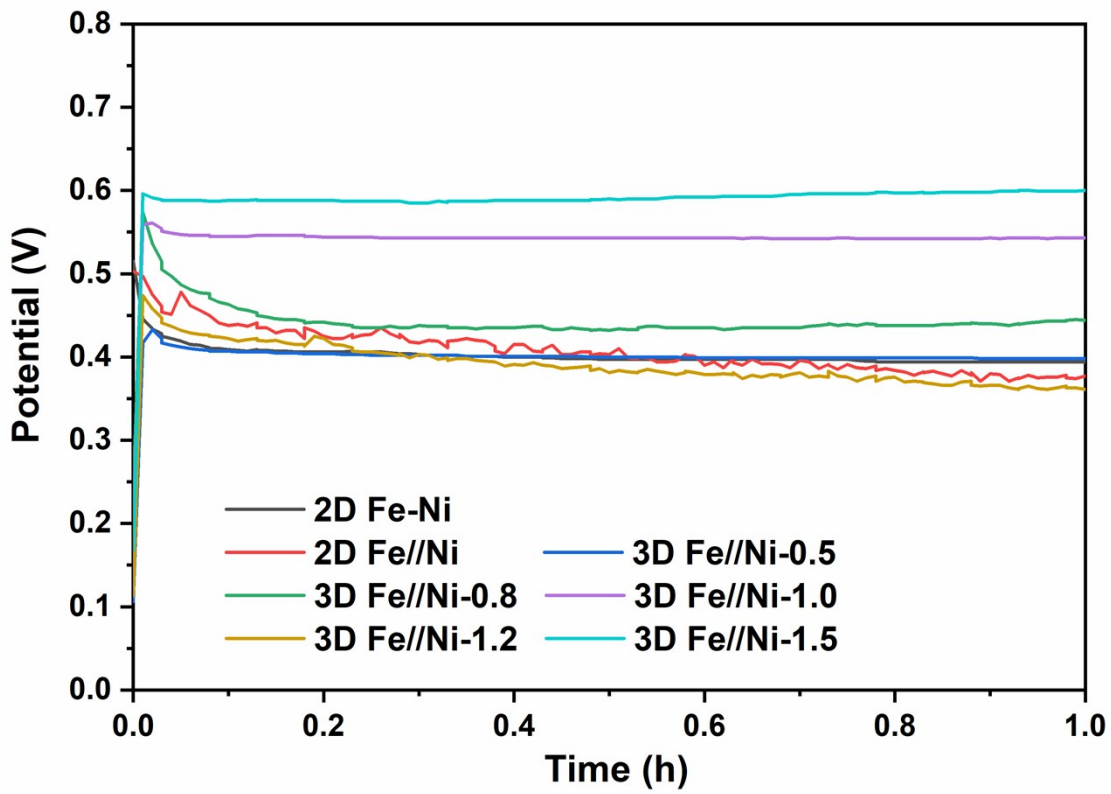

Figure S7 Galvanostatic charge curves of 2D Fe-Ni, 2D Fe//Ni, 3D Fe//Ni-X (0.5, 0.8, 1.0, 1.2, 1.5) electrodes at 10 mA cm^{-2} current density.

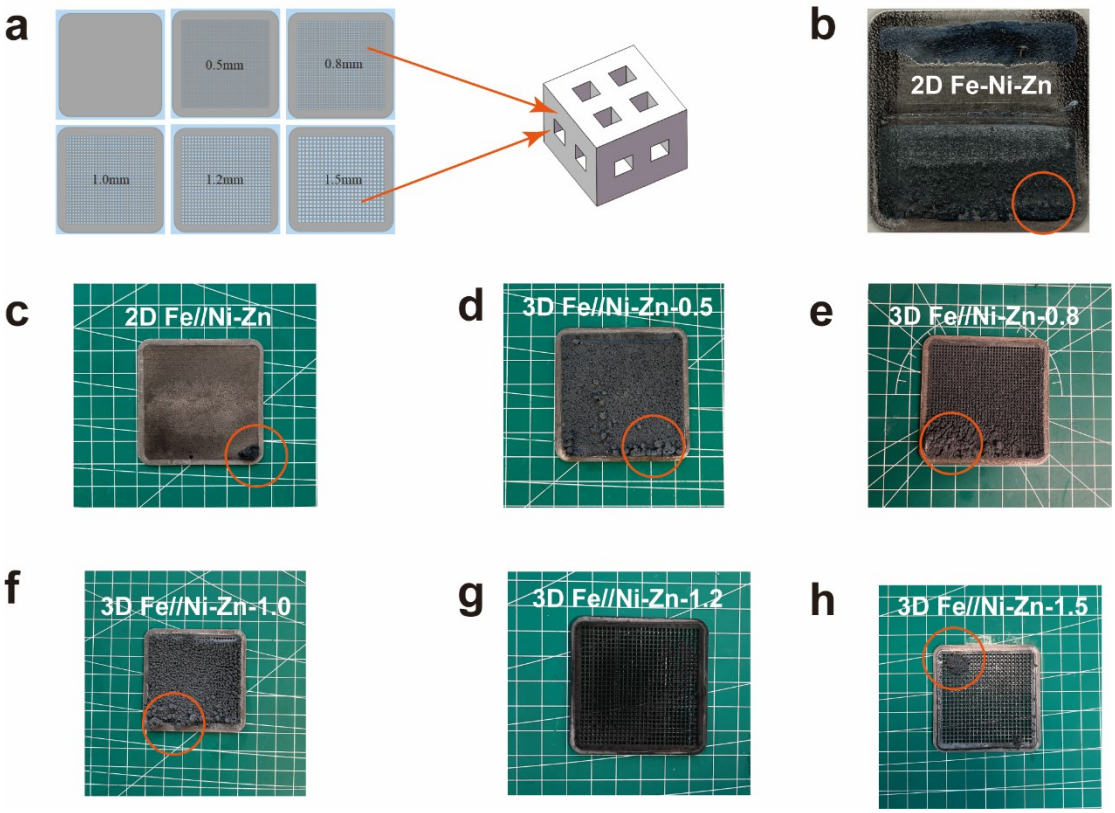

Figure S8 (a) Model drawings of 2D Fe-Ni and 3D Fe-Ni-X (0.5, 0.8, 1.0, 1.2 1.5) electrodes and cross-sections at any position of the 3D electrode. (b) 2D Fe-Ni-Zn cycle reaction 20 h after the electrode surface physical picture. (c) 2D Fe//Ni-Zn cycle reaction 180 h after the electrode surface physical picture. (d-h) 3D Fe//Ni-Zn-X (0.5, 0.8, 1.0, 1.2, 1.5) physical picture of the electrode surface after 300, 325, 400, 600 and 1050 h cyclic reactions, respectively.

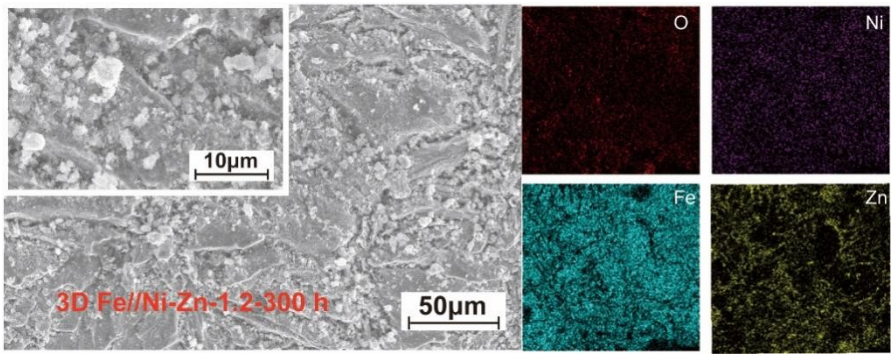

Figure S9 SEM morphology and EDX elemental distribution of 3D Fe//Ni-Zn-1.2 electrode after 300h of galvanostatic cycling.

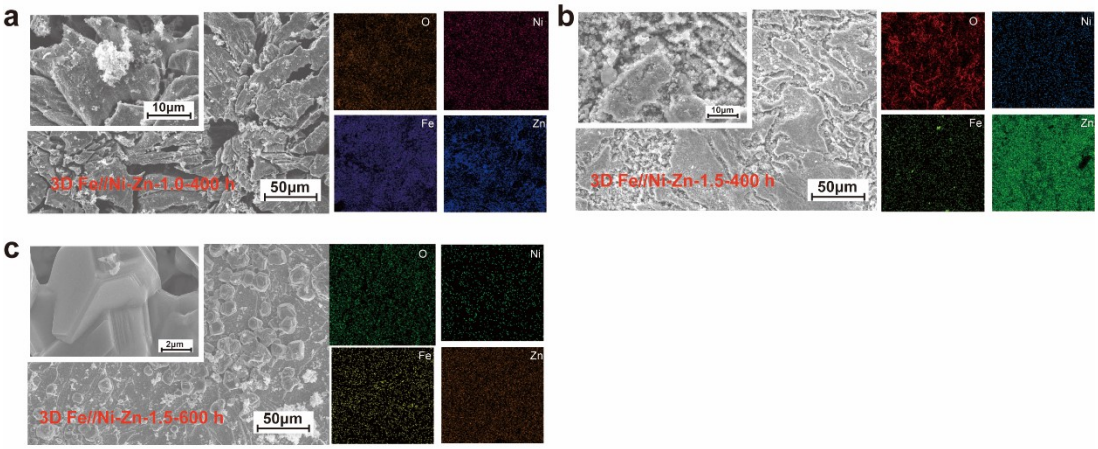

Figure S10 (a-b) SEM surface morphology and EDX elemental distribution of 3D Fe//Ni-Zn-X (1.0, 1.5) electrodes after 400h. (c) SEM surface morphology and EDX elemental distribution of 3D Fe//Ni-Zn-1.5 electrodes after 600 h.

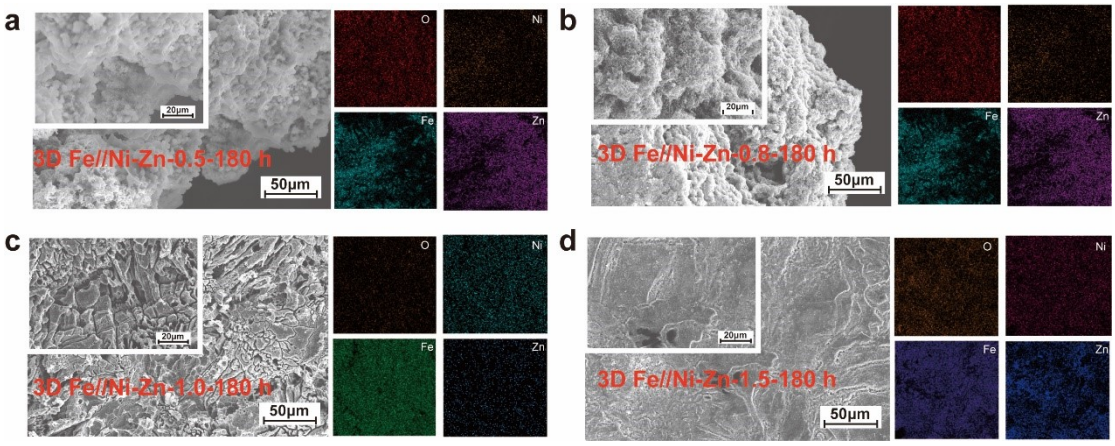

Figure S11 (a-d) SEM surface morphology and EDX elemental distribution of 3D Fe//Ni-Zn-X (0.5, 0.8, 1.0, 1.5) electrodes after 180 h.

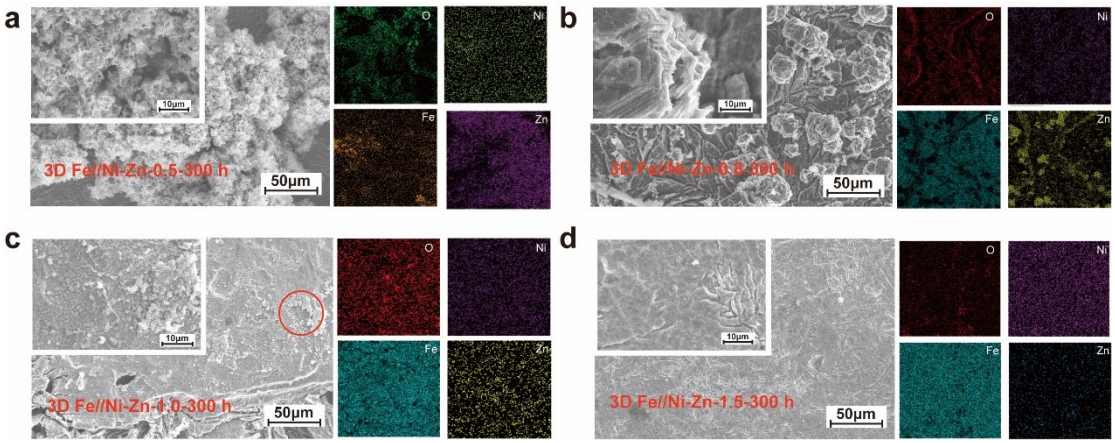

Figure S12 (a-d) SEM surface morphology and EDX elemental distribution of 3D Fe//Ni-Zn-X (0.5, 0.8, 1.0, 1.5) electrodes after 300 h.

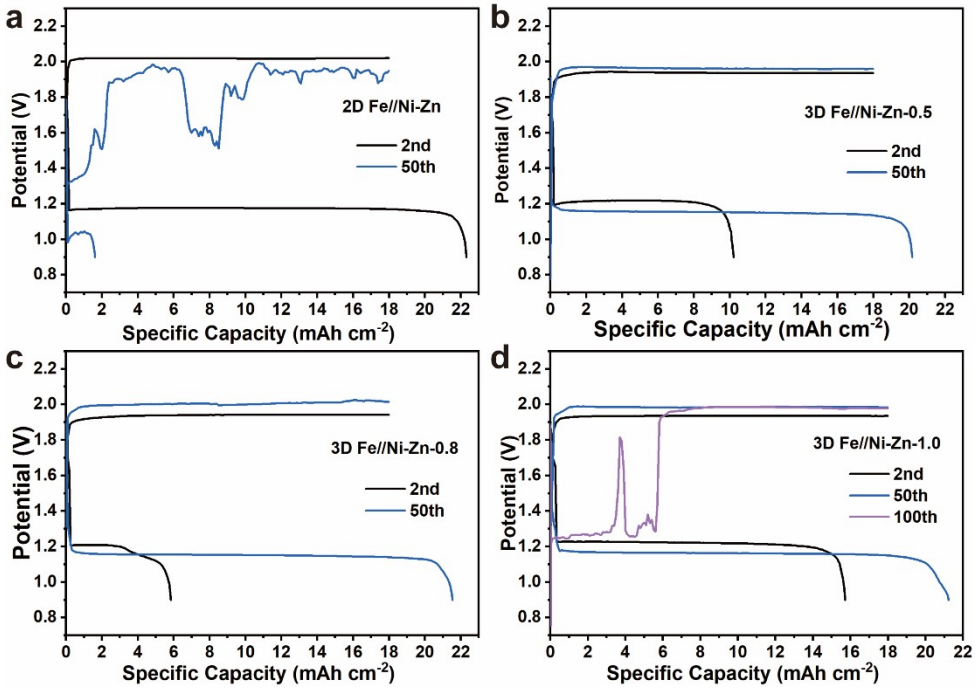

Figure S13 (a-c) The CV curves of 2D Fe//Ni-Zn, 3D Fe//Ni-Zn-0.5, 3D Fe//Ni-Zn-0.8 electrodes at the 2nd and 50th cycles, respectively. (d) 3D Fe//Ni-Zn-1.0 electrodes at the 2nd, 50th and 100th cycles.

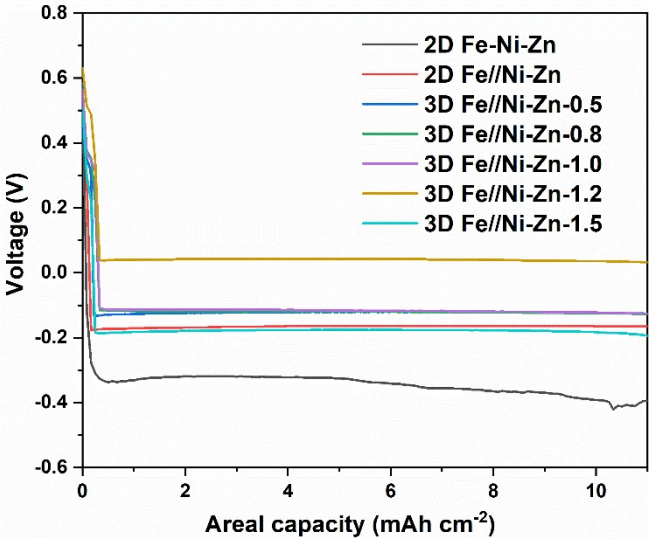

Figure S14 The potential profile of zinc deposition at 10 mA cm^{-2} current density.

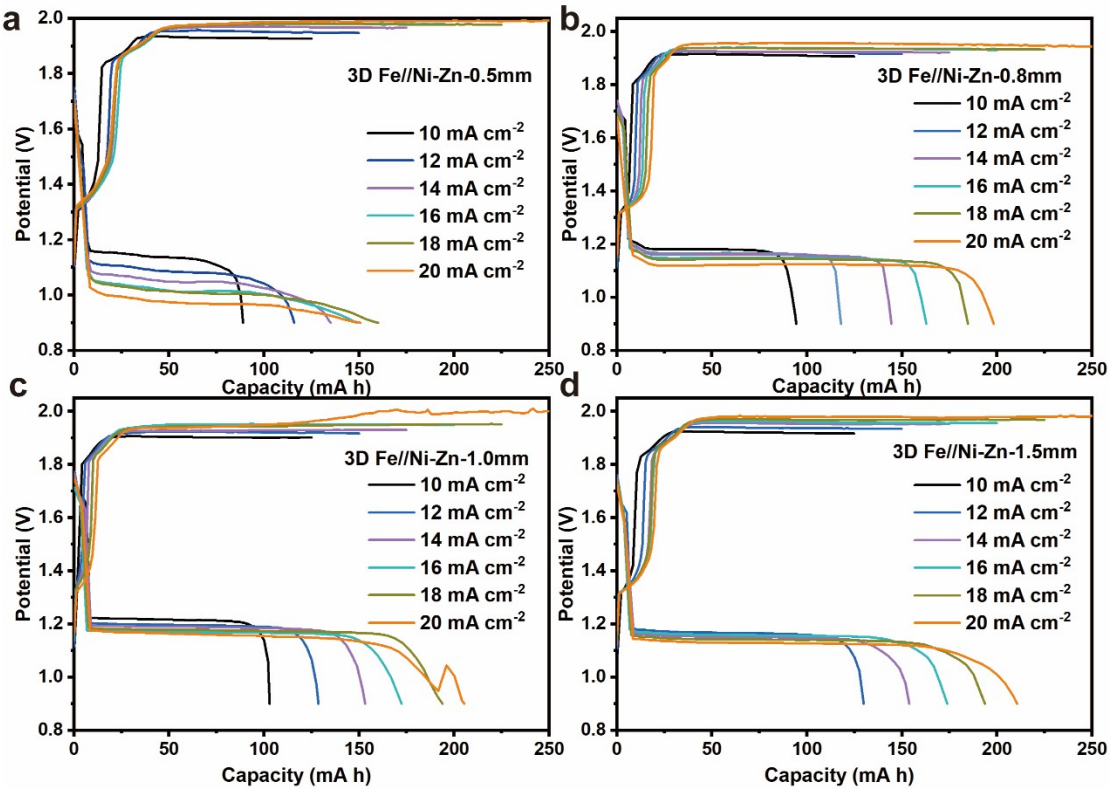

Figure S15 Voltage profiles of 3D Fe//Ni-X (0.5, 0.8, 1.0, 1.5) electrodes at different current densities.

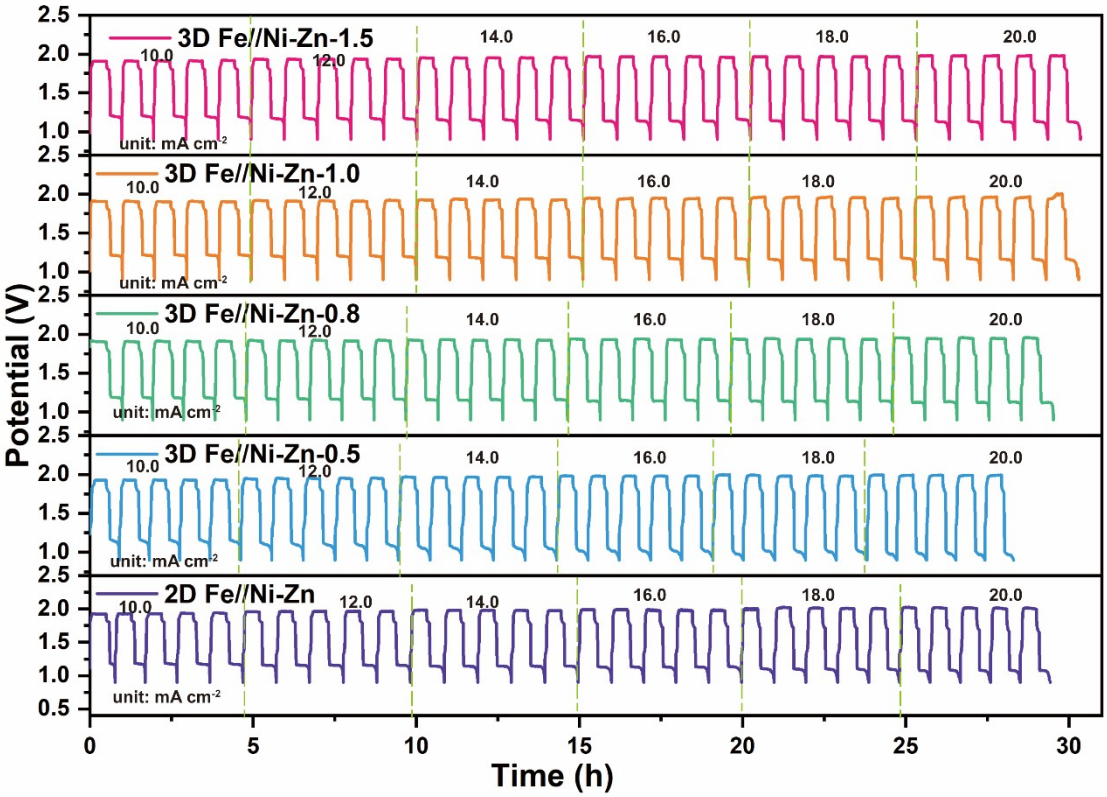

Figure S16 CV plots of 2D Fe//Ni-Zn and 3D Fe//Ni-X (0.5, 0.8, 1.0, 1.5) electrodes at different current densities.

Table S3 A summary of the electrochemical properties of other new zinc anode structures.

Zinc anode materials	Current density (mA cm^{-2})	Lifespan (h)	Ref.
Triple-gradient Zn anode	10	250	Adv Mater[2]
3DP-NC@Zn	1	380	Adv Energy Mater[3]
3D Ni-Zn	5	200	Adv Energy Mater
C-840/Zn	10	400	Adv Energy Mater[4]
3D Zn anode	0.5	350	Acs Sustain Chem Eng[5]
ZF@F-TiO_2	1	460	Nat Commun[6]
Zn–Cu Alloy	2	300	Small[7]
TZNC@Zn	1	450	Angew Chem Int Edit[8]
Zn micromesh	5	250	Adv Funct Mater[9]
ICZ anode	5	350	Nano Energy[10]
3D Fe//Ni-Zn-1.2	10	1050	This work

参考文献

1. Li, H., et al., *Fe–Ni Alloy Nanoclusters Anchored on Carbon Aerogels as High-Efficiency Oxygen Electrocatalysts in Rechargeable Zn–Air Batteries.* Small, 2021. **17**(36): p. 2102002.
2. Gao, Y., et al., *Stable Zn Anodes with Triple Gradients.* Advanced Materials, 2023. **35**(6): p. 2207573.
3. Zeng, L., et al., *3D Printing Architecting Reservoir-Integrated Anode for Dendrite-Free, Safe, and Durable Zn Batteries.* Advanced Energy Materials, 2022. **12**(12): p. 2103708.
4. Yuksel, R., et al., *Metal-Organic Framework Integrated Anodes for Aqueous Zinc-Ion Batteries.* Advanced Energy Materials, 2020. **10**(16): p. 1904215.
5. Kang, Z., et al., *3D Porous Copper Skeleton Supported Zinc Anode toward High Capacity and Long Cycle Life Zinc Ion Batteries.* Acs Sustainable Chemistry & Engineering, 2019. **7**(3): p. 3364-+.
6. Zhang, Q., et al., *Revealing the role of crystal orientation of protective layers for stable zinc anode.* Nature Communications, 2020. **11**(1).
7. Liu, B.T., et al., *Novel 3D Nanoporous Zn-Cu Alloy as Long-Life Anode toward High-Voltage Double Electrolyte Aqueous Zinc-Ion Batteries.* Small, 2020. **16**(22): p. 2001323.
8. Sun, P.X., et al., *Formation of Super-Assembled TiOx/Zn/N-Doped Carbon Inverse Opal Towards Dendrite-Free Zn Anodes.* Angewandte Chemie-International Edition, 2022. **61**(7).
9. Liu, H.Z., et al., *Ultrathin and Ultralight Zn Micromesh-Induced Spatial-Selection Deposition for Flexible High-Specific-Energy Zn-Ion Batteries.* Advanced Functional Materials, 2021. **31**(48): p. 2106550.
10. Yin, J., et al., *Regulating the redox reversibility of zinc anode toward stable aqueous zinc batteries.* Nano Energy, 2022. **99**: p. 107331.